Biofidelity Evaluation of the Hybrid-III 50th Male and the THOR-50M in Reclined Frontal Impact Sled Tests

Jeesoo Shin, John Paul Donlon, Rachel Richardson, Bronislaw Gepner, Jason Forman,
Martin Östling, Jason Kerrigan

Abstract With the development of highly automated vehicles, the automotive industry predicts more occupants will opt for reclined seating. This study aimed to evaluate the biofidelity of the Hybrid-III 50th Male and THOR 50th Male anthropomorphic test devices (ATDs) in a reclined frontal sled impact condition. Three tests per ATD were performed in a reclined condition previously used to test post-mortem human subjects (PMHS). ATD kinematics were captured using an optical 3D motion tracking system. Analogous anatomic points were defined relative to the rigid structure on the ATD corresponding to the anatomic structure of the PMHS, which permitted direct comparison of the kinematics of the ATDs and the PMHS. Qualitative biofidelity evaluation was conducted by comparing signals from the two ATDs to corresponding PMHS response corridors. Both ATDs exhibited good repeatability and similarities to the PMHS in some respects, but magnitudes and directions of other parameters were dissimilar. This was observed especially in the pelvis, where forward, rearward, and near-zero rotation were seen in the HIII-50M, the THOR-50M, and the PMHS, respectively. Maximum pelvis forward displacement also varied between the HIII-50M (100 mm), the THOR-50M (200 mm), and the PMHS (150 mm). Data and analysis from this study could become the basis for future biofidelity-augmenting ATD modifications.

Keywords Biofidelity, frontal impact, Hybrid-III, recline, THOR

I. INTRODUCTION

The imminent introduction of highly automated vehicles society-wide presents new challenges to occupant safety. In an autonomous driving system, the driver will no longer be required to actively operate the vehicle at all times [1-3]. Current state-of-the-art restraint systems have primarily been developed with the intention of protecting occupants in a forward-facing, upright posture. As such, the industry expects that one novel consideration involves occupants seated in forward-facing postures with seatback recline angles [4-6]. Previous experimental and computational studies have suggested that the increase in seatback recline angle leads to an increased risk of submarining, a phenomenon wherein the lap-belt passes over the iliac crest of the pelvis and loads the abdomen, which can cause abdominal injuries [7-8]. Submarining was observed in reclined occupants using restraint systems both with [9-13] and without lap-belt pre-tensioning [14]. These studies show that occupant kinematics and the effectiveness of countermeasures are affected by recline angle.

Advancements in human body models (HBMs) and computational simulations have been and continue to be used to assist in facilitating injury countermeasure design [15], but prototype evaluation and performance assessment still relies on the use of ATDs [16-19]. The two most commonly used ATDs in frontal impact conditions are the Hybrid-III Mid-Size Male (HIII-50M) and the Test device for Human Occupant Restraint Mid-Size Male (THOR-50M) [20]. Biofidelity assessment of ATDs is typically completed through a comparative analysis between the responses of ATDs and post-mortem human subjects (PMHS); this has been conducted for the Hybrid-III and the THOR in traditional, i.e., upright, forward-facing, seating postures [20-21]. However, no study into the biofidelity of the two ATDs in a reclined posture has been performed. This study aimed to characterise the response and evaluate the biofidelity of the HIII-50M and THOR-50M ATDs in a reclined frontal sled impact condition, with a focus on kinetic boundary conditions and kinematic responses of the surrogates.

J. Shin is a MS student in Mechanical and Aerospace Engineering (+1-434-297-8052 / jeesoo@virginia.edu), J. P. Donlon is a Senior Research Specialist, R. Richardson is a PhD student in Mechanical and Aerospace Engineering, B. Gepner is a Research Scientist, J. Forman is a Principal Scientist, and J. Kerrigan is an Associate Professor of Mechanical and Aerospace Engineering at the University of Virginia Center for Applied Biomechanics, USA. M. Östling is a Senior Research Specialist at Autoliv Development AB, Vårgårda, Sweden.

II. METHODS

Three 50 km/h frontal sled tests per ATD were performed (Table 1) using a simulated vehicle occupant environment or "buck" (Figure 1). Test conditions, such as sled pulse, subject positioning, and restraint type, were matched as closely as possible to those described in [22-23], which seated PMHS in a reclined posture. Further mentions of PMHS or PMHS tests refer to the tests and associated results presented in [23]. The upper extremities of the PMHS were amputated at mid-forearm [23], so the forearms of the ATDs were omitted and a point mass of 0.64 kg was secured at each elbow to match the average residual forearm mass.

TABLE I
TEST MATRIX FOR BIOFIDELITY EVALUATION TESTS.

Test Number	Subject	Sagittal Torso Angle	Pelvis Angle
S0702	HIII-50M	48° recline	42°
S0705	HIII-50M	49° recline	42°
S0706	HIII-50M	48° recline	41°
S0709	THOR-50M	47° recline	42°
S0710	THOR-50M	49° recline	44°
S0711	THOR-50M	49° recline	43°

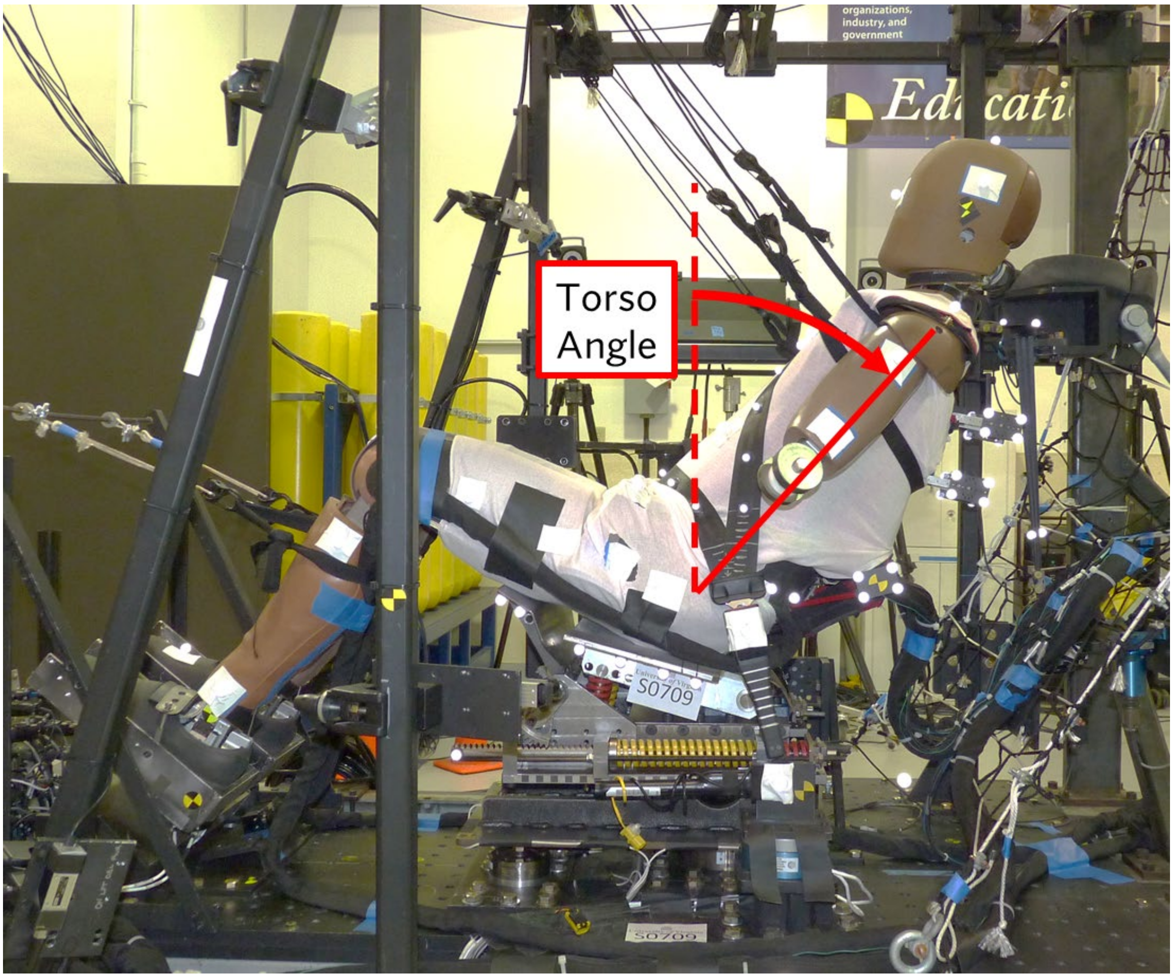

Fig. 1. Simulated vehicle occupant environment (buck); sagittal torso posture defined (with respect to vertical).

Restraint System

A concept restraint system that includes a 4 kN shoulder-belt load limiter, a crash locking tongue, and pretensioners at the buckle, lap-belt retractor, and shoulder-belt retractor was used [13][22]. In the PMHS tests, the lap-belt retractor and the shoulder-belt retractor positions were not changed among subjects and the D-ring was adjusted laterally to be 152 mm outboard of the right external auditory meatus and adjusted vertically to achieve an angle of 12° along the webbing from the shoulder to the D-ring. In the ATD tests, the lap-belt retractor and shoulder-belt retractor positions were likewise not changed, but the D-ring was instead placed at the average position of the PMHS tests. The shoulder-belt was routed over the middle of the clavicle and the middle of the sternum, and the lap-belt was routed as low as possible across the abdomen, inferior to the anterior superior iliac spines (ASIS). The buckle, lap-belt, and shoulder-belt pretensioners were activated at 3 ms, 10 ms, and 10 ms, respectively.

Test Measurements

Seat loads (forces and moments) were measured through three load cells located underneath the semi-rigid seat. Footpan and buckle loads were measured similarly with load cells attached beneath the footpan and buckle, respectively. Seat, footpan, and buckle forces and moments were inertially compensated to eliminate the contribution of the sprung mass to the measured loads. Both shoulder-belt and lap-belt forces were measured through belt tension gauges located between the D-ring and the ATD's shoulder and the lap-belt retractor and the ATD's right hip, respectively. An optoelectronic stereophotogrammetric system (Vicon, Centennial, CO, USA) measured three-dimensional motions of spherical markers attached to the buck, seat, seatbelt, and subject to track subject kinematics. A coordinate system (CS) was defined on the buck to describe position measurements and subject motions. The buck CS had its origin at the right rear top corner of the seat's rigid frame (Figure 2). The axes of the buck CS accorded with the Society of Automotive Engineers (SAE) convention: positive Z-axis direct downward, positive X-axis directed forward, and positive Y-axis directed rightward [24].

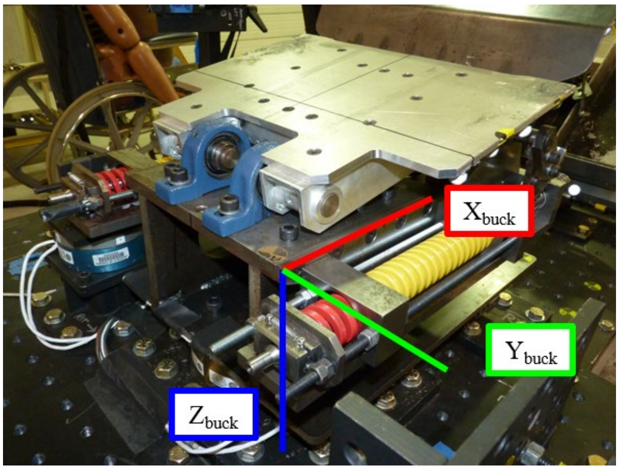

Fig. 2. Buck coordinate system

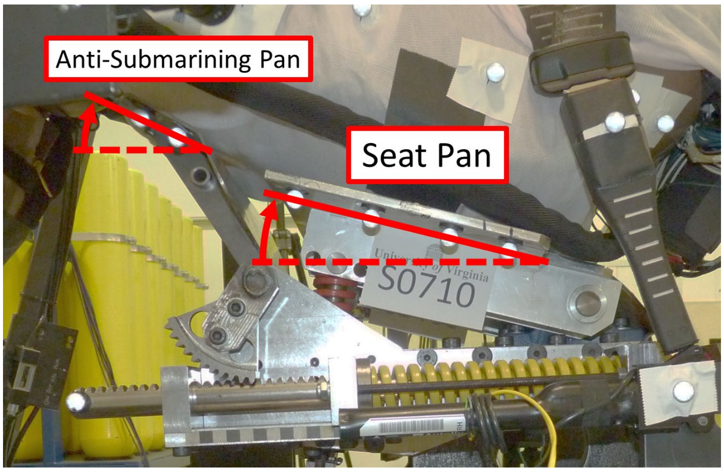

Fig. 3. Rotation measurements for the anti-submarining pan and seat pan

Rotations for the seat pan and the anti-submarining pan were measured by defining the angle between the line segment connecting rigidly fastened motion tracking markers underneath the respective surfaces and the horizontal (Figure 3). Angular displacement was then calculated by debiasing the rotation time-history such that the angles of the seat pan and the anti-submarining pan were 0° at time = 0 ms.

Buckle displacement (or deflection) was defined as the change in distance between a marker placed on the buckle and a marker placed on the buckle base (Figure 4A). Shoulder-belt pay-in/pay-out was defined as the change in distance between a marker placed on the D-ring and a marker placed on the webbing between the D-ring and the shoulder (Figure 4B). Lap-belt pay-in/pay-out was defined as the change in distance between a marker placed on the lap-belt (lateral to the outboard thigh) and a pseudo-marker defined 50 mm inboard of a marker placed on the anchor (Figure 4C, Figure 4D). For all belt displacement measurements, a decrease in point distance, i.e., pay-in, was defined as negative and an increase in point distance was defined as positive.

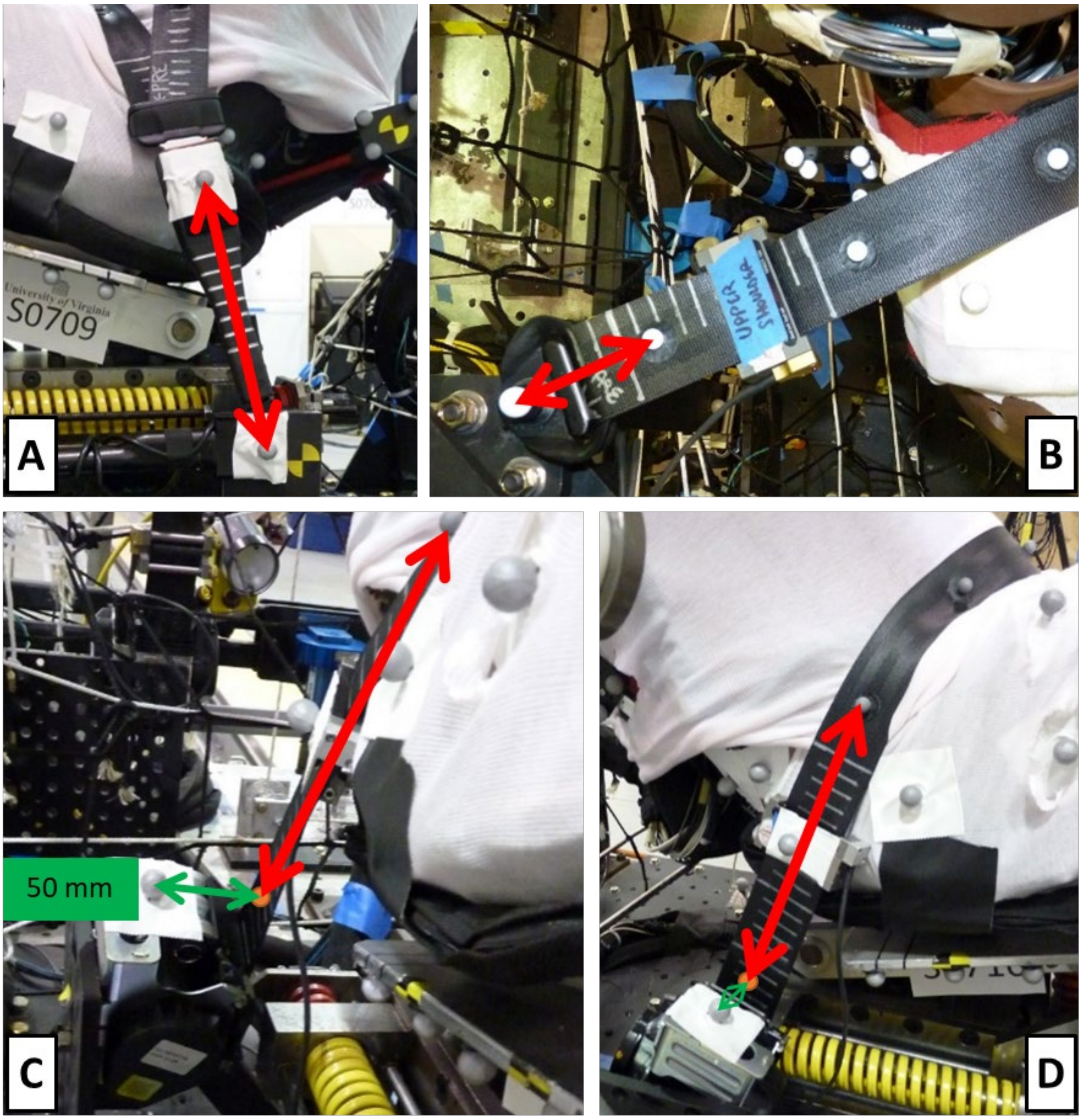

Fig. 4. Displacement measurements for the buckle (A), shoulder-belt (B), and lap-belt (C, D).

Motion-Capture Data

Rigid arrays of markers were designed and rigidly attached to structures (pelvis, spine, and head) of the ATDs to permit calculation of the structures' motion. A least-squares pose estimator was used to minimise error in the calculated motion of the array [25]. Local coordinate systems of the ATDs' underlying structures were defined to permit rigid-body coordinate transformations from the marker array to the internal structure of the ATDs (Figure 5; Appendix B). The motion of the marker array was then used along with ATD drawings and digitization of the array assemblies to calculate the motion of the underlying structure using a rigid-body coordinate transformation analysis [25]. Points on the ATDs' internal structures corresponding to anatomic points on the PMHS were calculated by adapting the method outlined in [26] (Figure 5). The general steps of this method are:

1. Position PMHS and ATDs in the same gross posture and position relative to the buck
2. Measure the positions of the internal anatomy of the PMHS relative to the buck
3. Measure the positions of the internal structures of the ATDs relative to the buck
4. Calculate the positions of the PMHS anatomic points relative to the ATD structures

The motions of the ATDs during the test could then be described by the motions of these pseudo-anatomic points, which permitted direct comparison with the motions of the corresponding anatomic points on the PMHS.

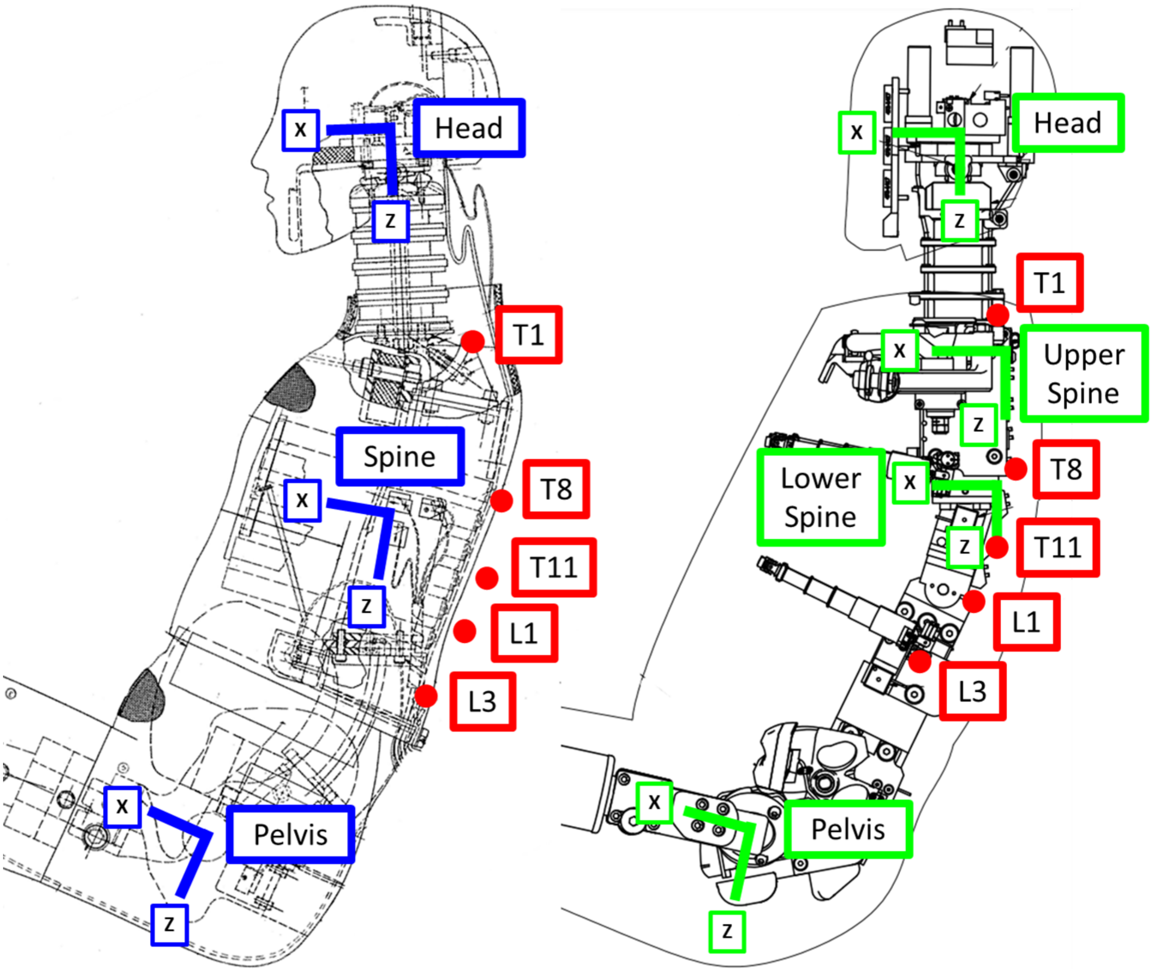

Fig. 5. ATD structure coordinate system. Left: HIII-50M; Right: THOR-50M.

Step 1 was completed by establishing three principal quantitative targets for subject positioning: the position of the hip-point (H-point), the recline angle of the torso, and the orientation of the pelvis. The X-coordinates of the ATDs' H-points were matched with the X-coordinate of the PMHS' H-point (+130 mm (HIII-50M) and +150 mm (THOR-50M) relative to the buck CS) [27]; the Z-coordinates were not controlled due to differences in posterior pelvis flesh thickness. Compared to the PMHS, the average Z-coordinate of the H-points of the HIII-50M and the THOR-50M was +10 mm (lower) and -35 mm (higher) in the buck CS, respectively. The recline angle of the torso was defined as the angle in the sagittal plane of the line connecting the H-point and the acromion [23] (Figure 1). While the acromion of the THOR-50M is well defined, that of the HIII-50M is not well defined, so an *acromion tool* was fabricated to facilitate digitisation of the HIII-50M acromion (Appendix C). The target recline angle of the torso was 50° from the vertical (Table 1). The orientation of the pelvis was described through the pelvis angle, defined as the *Notch Angle*, the angle in the sagittal plane of the line connecting the midpoint of the ASIS and the midpoint of the Anterior Inferior Iliac Spines (AIIS) [28]. The Notch Angle may better describe sensitivity of pelvis restraint kinematics and kinetics to pelvis orientation [28]. The target pelvis angle was between 40° and 49° from the horizontal. To achieve the target pelvis angle and recline angle of the torso simultaneously with the THOR-50M, the lumbar pitch joint was set to the *super-slouched* position (12°).

Step 2 was performed by [23] using the motion-capture measurements of the PMHS in their initial (pre-impact) position. For each PMHS, [21] calculated the initial positions of the centres of the T1, T8, T11, L1 (in three PMHS), and L3 vertebral bodies. Step 3 was completed using the motion-capture measurements of the ATDs in their initial (pre-impact) position. Step 4 was performed as described in [26] using a coordinate system transformation.

Identification of Pseudo-Anatomic Points on the ATDs

For the vertebrae, coordinate system transformations yielded pseudo-anatomic points relative to the rigid structure on the ATD corresponding to the anatomic structure of the PMHS (Figure 5; Table 2).

TABLE II
ATD ANATOMICAL LANDMARK LOCATIONS RELATIVE TO RESPECTIVE ATD COMPONENT COORDINATE SYSTEMS.

ATD	Component	Anatomical Landmark	X (mm)	Y (mm)	Z (mm)
HIII-50M	Spine	T1	-55.6	18.1	-183.4
	Spine	T8	-110.1	18.3	-34.2
	Spine	T11	-108.4	20.6	44.0
	Spine	L1	-89.6	26.4	106.2
	Spine	L3	-61.1	28.4	178.3
THOR-50M	Upper Spine	T1	3.8	-34.0	-38.2
	Lower Spine	T8	-20.1	-21.9	-14.6
	Lower Spine	T11	4.6	-18.7	59.7
	Lower Spine	L1	41.2	-13.0	113.4
	Lower Spine	L3	89.7	-11.5	173.9

III. RESULTS

The responses of the ATDs were plotted against the corresponding PMHS corridors [23] for the signals outlined in Appendix B for qualitative biofidelity assessment (Appendix D).

Environment Loads

The HIII-50M and THOR-50M displayed repeatable environment load responses, with minimal variation among each ATDs' three tests (Appendix D: Figure D2). Both ATDs showed higher maximum lap-belt forces than the PMHS, though the peak force for the HIII-50M falls within the PMHS corridor (Appendix D: Figure D2). The THOR-50M peaks a few milliseconds earlier than the PMHS, at around 8.5 kN, and the HIII-50M peaks a few milliseconds earlier than that, at around 8 kN. Differences in shoulder- and lap-belt force magnitude between the ATDs and the PMHS begin to occur just after pretensioning (approximately 15 ms). Both ATDs also showed higher maximum shoulder-belt forces (Appendix D: Figure D2). The HIII-50M's shoulder-belt force peaked earliest, at around 4.2 kN, followed by the THOR-50M (4 kN) and the PMHS (3.6 kN). The shoulder-belt force decreased in the same order as well. Buckle forces were again higher in magnitude for the ATDs, with the peak force occurring earlier for the two ATDs than the PMHS (Appendix D: Figure D2). For the THOR-50M, the buckle force increased a second time at around 90 ms. Seat forces in the X- and Z-directions for the two ATDs generally fell within the PMHS corridors, while footpan forces were greater in the ATDs than the PMHS (Appendix D: Figure D2).

Whole Body Kinematics

High-speed video images from tests on all three surrogates provide a basis to perform generalised comparison across the surrogates (Figure 6). As displayed in their environment load responses, both ATDs exhibited good repeatability in kinematic signals across key measured regions of the body (Appendix D: Figures D3-D6). An overall trajectory plot (Figure 7) shows that the PMHS mean generally falls between the HIII-50M's and the THOR-50M's trajectories, particularly for the vertebral bodies. The PMHS mean head trajectory falls closer to that of the THOR-50M, both with less vertical displacement than the Hybrid-III. As a whole, the THOR-50M's lumbar spine and pelvis appeared to translate forward more than either the HIII-50M or PMHS.

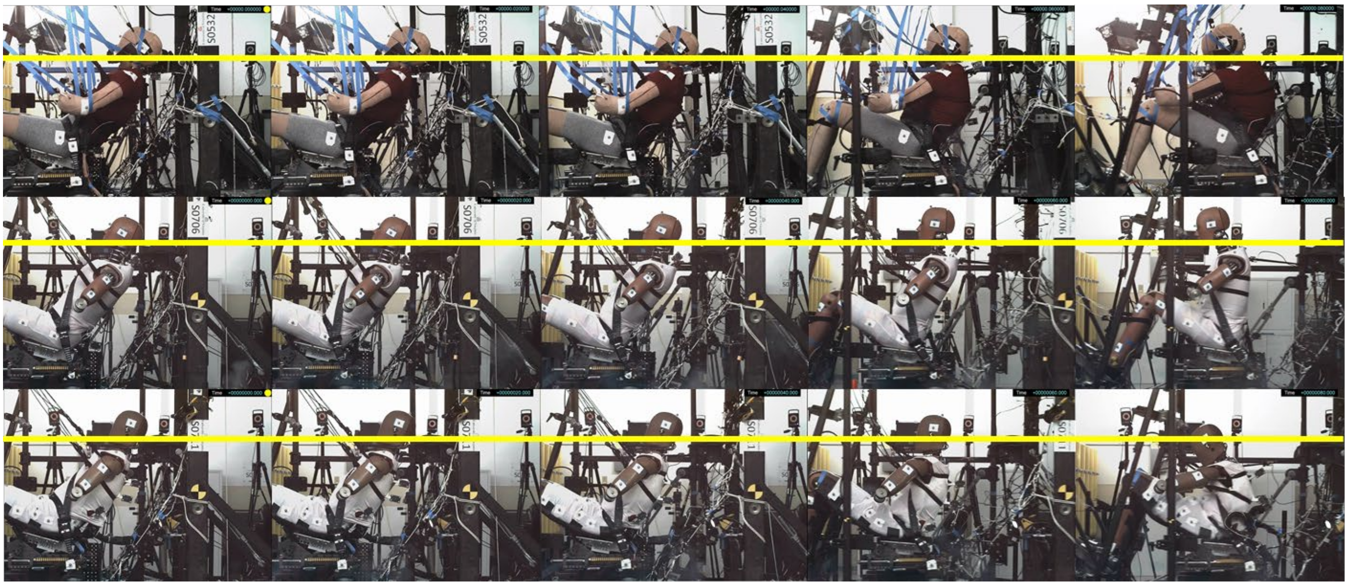

Fig. 6. Comparison of PMHS, HIII-50M, and THOR-50M, from top to bottom, in a reclined frontal sled impact condition. Snapshots are taken at t = 0, 20, 40, 60, and 80 ms. Peak forward pelvis displacement of the PMHS and ATDs occurs between 65 and 75 ms. Yellow lines indicate initial vertical position of head centre of gravity.

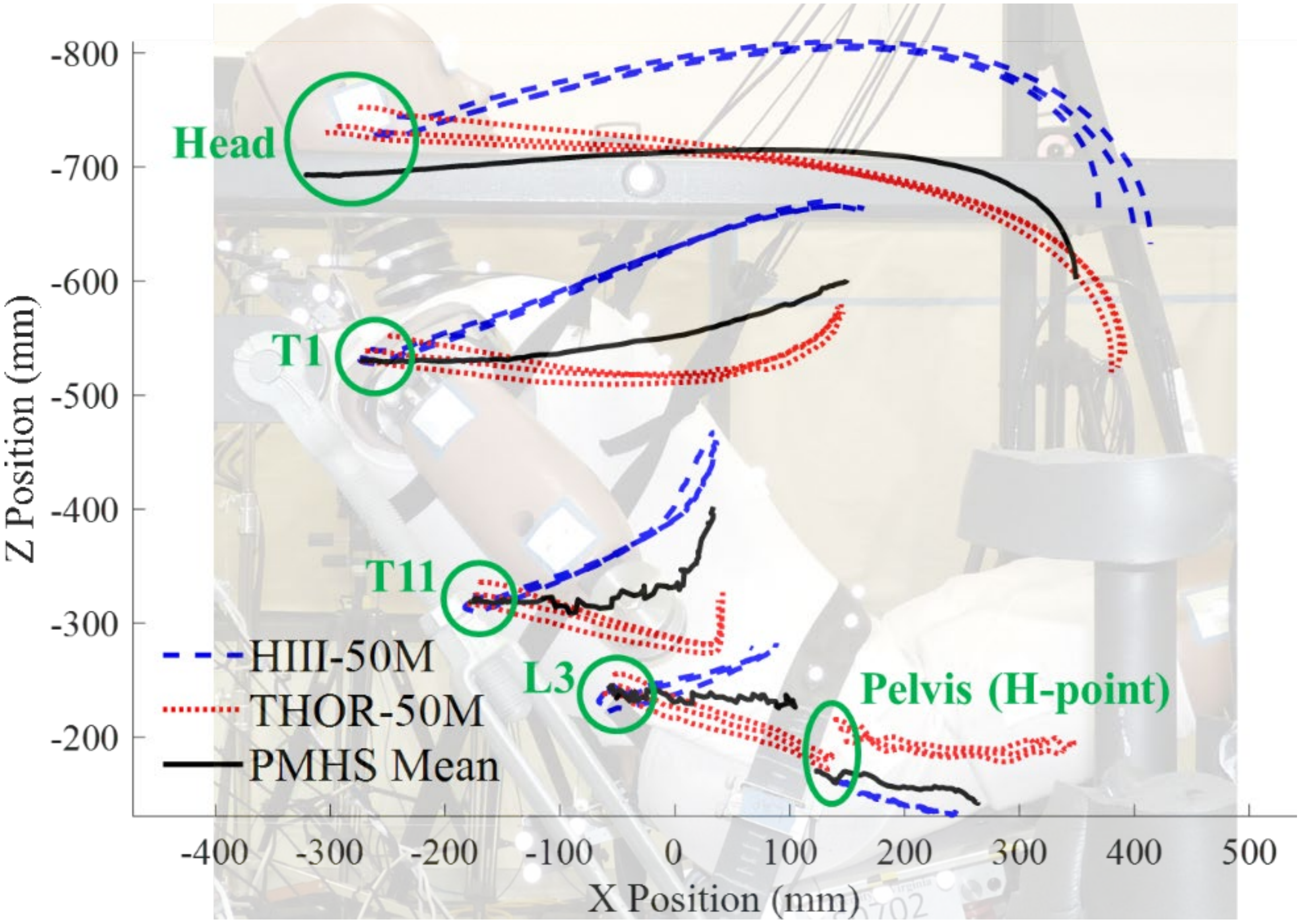

Fig. 7. Sagittal plane trajectories of the head, T1, T11, L3, and pelvis (H-point) for the HIII-50M, THOR-50M, and PMHS displayed until respective peak forward excursions.

Pelvis Kinematics

Forward pelvis excursion of the PMHS peaked at around 140 millimeters at 70 milliseconds (Appendix D: Figure D6). The THOR-50M showed greater maximum pelvis forward excursion, at around 185 millimeters, and peaked a couple of milliseconds after the PMHS. In contrast, the HIII-50M showed lower maximum pelvis forward excursion, at around 100 millimeters, and peaked about 7 milliseconds prior to the PMHS. The PMHS exhibited low negative, or forward, pelvis pitch, at about 5 degrees in magnitude, prior to peak pelvis excursion, which occurred at around 70 milliseconds. The HIII-50M exhibited forward pelvis pitch, 20 to 25 degrees, while the THOR-50M exhibited a pelvis pitch in the opposite direction (positive and rearward) of the HIII-50M and the PMHS with similar magnitude to the Hybrid-III. Neither ATD submarined in any test, whereas one of the four PMHS submarined.

Thoracolumbar Spine Kinematics

Forward displacement of the pseudo-anatomic landmarks on the thoracic spine (T1, T8, T11) of both ATDs generally fell within their respective PMHS corridors (Appendix D: Figures D4 & D5). Some greater differences in lateral and vertical displacements for the thoracic spine were evident. Generally, the PMHS corridors for vertical displacement of the thoracolumbar spine (T1, T8, T11, L1, L3) fell between the responses of the THOR-50M and the HIII-50M, with the THOR-50M displaying greater peak vertical displacement and the HIII-50M less than the PMHS. The lumbar spine (L1, L3) of both ATDs displayed a kinematic response more closely resembling their pelvis kinematics, with the THOR and the Hybrid-III falling along the upper and lower bounds of the PMHS corridors, respectively. In general, the THOR displayed the most spinal flexion, followed by the PMHS and then the HIII-50M.

Head Kinematics

Both the HIII-50M and THOR-50M displayed similar forward head trajectories, with THOR-50M’s peak forward head displacement occurring about 10 ms earlier and about 30 mm greater in magnitude (Appendix D: Figure D3). The PMHS peak forward head displacement occurred at a similar time to the HIII-50M’s, with a magnitude between that of the HIII-50M and the THOR-50M. Lateral head motion of the HIII-50M matched that of the PMHS, while the THOR-50M's head moved in the opposite direction: the heads of the Hybrid-III and the PMHS displace approximately 20 mm outboard, or rightwards, with respect to the occupant, by the time of maximum forward displacement (110 ms), while the THOR-50M's head remains centred until maximum forward displacement, after which the head proceeds to move inboard during rebound. HIII-50M’s vertical head displacement was similar to that of the PMHS, moving upwards (HIII-50M more than PMHS) and then downwards, but the THOR-50M's head only move downwards.

IV. DISCUSSION

This study provides a qualitative biofidelity evaluation of the HIII-50M and THOR-50M ATDs in a reclined frontal sled impact condition. While there are numerous corridors presented in the literature [23], biofidelity evaluation was conducted using a subset of corridors believed to be most important for ATD and HBM evaluation (Appendix A). Data that was captured in both the ATD and PMHS experiments were the subject of comparison, including kinetic boundary conditions, such as belt and seat loads, and kinematic responses of the surrogates. That said, there are other metrics, including local accelerations and angular rates, that are not compare directly in this study. These data from the ATD tests will be included in a subsequent paper.

Overall, both THOR-50M and HIII-50M showed good repeatability, but mixed results in terms of biofidelity, with neither vastly outperforming the other. This is not consistent with findings from a previous study that assessed the biofidelity of Hybrid-III and THOR in an upright posture, where THOR-50M displayed a more biofidelic response than HIII-50M in a frontal sled test condition [21].

Biofidelity Evaluation

The condensed list of signals from which biofidelity was evaluated includes all boundary kinetic signals (belt, seat, and footpan forces), seat pan and anti-submarining pan rotation, restraint system responses (belt pay-in/pay-out) and surrogate kinematic responses in the form of displacements captured by 3D motion tracking. For biofidelity evaluation, displacements captured by 3D motion-tracking are favored over sensor-based kinematics, i.e., integration of accelerations and angular rates, since the response traces and their associated corridors tend to be less noisy, more accurate, and show better repeatability among tests [29]. Since Y-direction displacements of the lower spine and pelvis were of small magnitude relative to the X- and Z-directions, these signals were not included. Lastly, local angular rate (Y-axis), and global rotation (Y-axis) corridors are included for the head and pelvis since they capture major differences in response between the ATDs and PMHS.

Biofidelity corridors aim to represent the measured mechanical behavior of a sample of human subjects (volunteer or PMHS). Reference [23] calculated corridors using two different methods: a *simple* method taking the mean and standard deviation across subjects at each time-step; and the normalised arc-length parametrisation (NALP) method of Perez-Rapela et al. [30]. The NALP method may better represent a sample of responses which have similar shape but different phase, but it requires selection of (at least) two homologous points on each response. Therefore, the *simple* method may suffice for biofidelity evaluation for responses which have different shape or similar shape, or which lack appropriate corresponding points. Appendix B lists which form of corridor was selected for each response compared. A quantitative biofidelity metric, such as CORrelation and Analysis (CORA) or the Biofidelity Ranking System (BioRank), was not applied as part of the evaluation. This is because the aim of this study was not to point out, through a single number, which ATD is better, as the ranking would be sensitive to the number and type of signals included, but to portray the differences of the ATDs' responses to the PMHS responses and suggest directions for further developments to either ATD and restraint systems.

Belt Forces

Maximum lap- and shoulder-belt forces were greater in both ATDs than the PMHS. However, when considering impulse, the area under the curve for a force versus time curve, the results are more comparable. Peak lap-belt force for the HIII-50M falls just within the upper bound of the PMHS corridor, but the HIII-50M's lap-belt force begins to unload earlier than the PMHS. Similarly, peak lap-belt force for the THOR-50M falls just above the PMHS corridor, but the loading phase after pre-tensioning occurs later than the PMHS. Peak shoulder-belt force was greatest in the HIII-50M, but the HIII-50M's shoulder-belt force unloaded earliest. This trend continued with the THOR-50M and the PMHS, with the PMHS displaying the lowest peak shoulder-belt force and unloading last. In almost all belt load cases, a higher peak force was paired with a reduced duration, leading to similar impulses. These slight differences in signals between the ATDs and the PMHS may be caused by a variety of factors, including, but not limited to, flesh compliance and belt webbing-flesh engagement.

Pelvis

Pelvis motion, specifically forward excursion (displacement in the X-direction) and pitch (rotation about the Y-axis) varied widely between the two ATDs and even between each ATD and the PMHS. For those two key signals, an interesting phenomenon wherein the HIII-50M and the THOR-50M signals fall on either side of the PMHS corridor occurs. The two signals not only fell on either side of the corridor, but the signals' peak values also differed from the PMHS average by an approximately similar magnitude. It is evident that the HIII-50M pelvis translates forward less and pitches forward more than the PMHS pelvis whereas the THOR-50M pelvis translates forward more and pitches rearward. This wide deviation indicates that the pelvis design of current ATDs can be improved upon to provide a more biofidelic response in the reclined condition. Some potential causes for the differences in pelvis motion may be pelvic flesh stiffness, pelvic geometry, and interaction with the seat, but future work should investigate the source of the divergence.

The PMHS tests resulted in localised compressive fractures of the outboard-side iliac wing in two of the three non-submarining tests [23]. Such injuries may not be common in the current vehicle fleet, but they may become more common if occupant restraint relies more on the seatbelt as opposed to the combination of restraints typically used in current vehicles, i.e., airbag, knee bolster. Interpretation of the current dataset is limited to observations of only the THOR-50M and is as follows:

1. The local X-component of ASIS force was never greater than the lap-belt force (Figure 8, left); this is consistent with prior work [28] and indicates .
2. The ASIS moment about the local y-axis was always negative (Figure 8, right); this indicates that the lap-belt engages the pelvis low on the ASIS, which may explain why submarining did not occur.

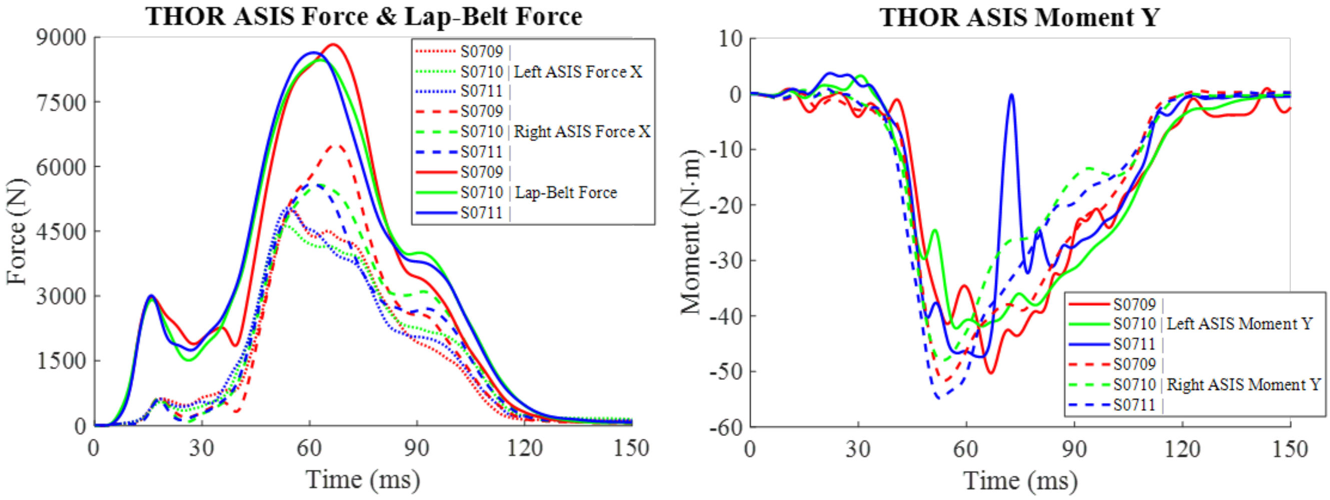

Fig. 8. Left and right ASIS forces in the x-direction compared to lap-belt force for THOR-50M (left) and left and right ASIS moments about the y-axis for THOR-50M.

Thoracolumbar Spine

Simulations of reclined occupants in frontal crashes predicted high compression and flexion of the lumbar spine [31], and L1 burst/compression fractures were observed in two of the four PMHS tests [32]. This suggests the need for an injury risk prediction metric for reclined ATDs in frontal impacts. Differences were observed between the two ATDs in the spine force along the Z-axis and spine moment about the Y-axis signals (Figure 9). Interpretation of these differences is confounded by differences in the location of compliant elements along the spine, differences in pelvis motion, and load cell location (THOR-50M's load cell is above the flexible lumbar element while HIII-50M's is below). This discrepancy should be resolved before an injury risk prediction metric is developed.

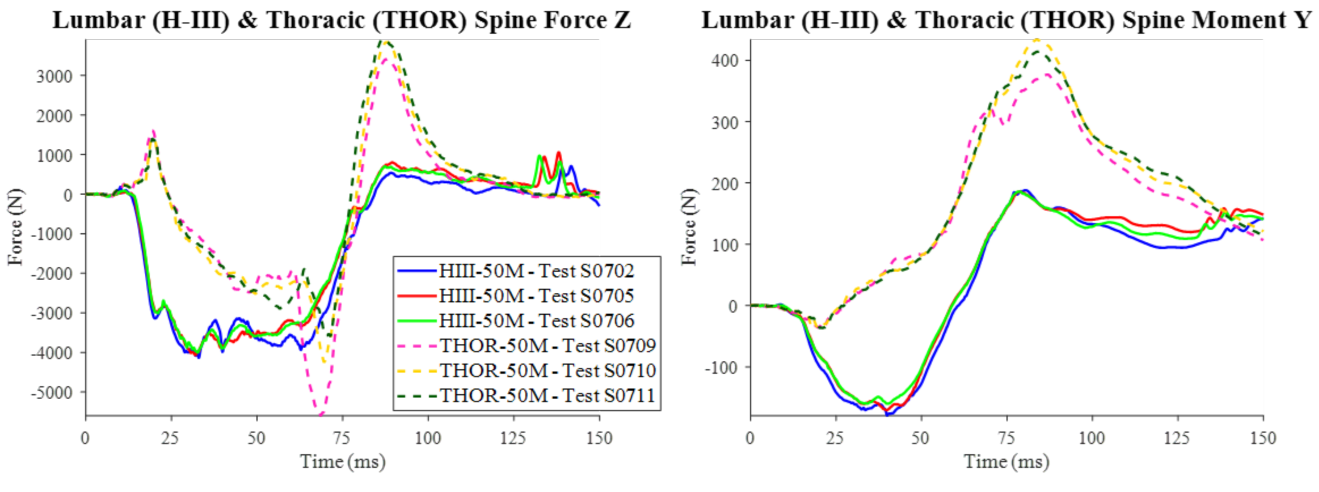

Fig. 9. Axial force (left; positive indicates tension) and y-axis bending moment (right; positive indicates flexion) for the lumbar spine (HIII-50M, S0702, S0705 & S0706) or for the thoracic spine (THOR-50M, S0709-S0711).

Head

Forward head trajectory was similar across all three surrogates despite large differences in pelvis motion. Therefore, it is likely that head forward displacement in this configuration is independent of pelvis motion. Despite similar mass and stature among PMHS and ATDs, responses measured all the way up the kinematic chain from the pelvis to the head indicate that the ATDs do not behave the same as the PMHS. For example, shoulder-belt payout of the Hybrid-III exceeded that of the PMHS, which in turn exceeded that of the THOR-50M (HIII-50M > PMHS > THOR-50M); while the order of magnitude was opposite for the head forward displacement (THOR-50M > PMHS > HIII-50M). Further factors could include neck compliance, upper thoracic compliance, and chest deflection. Therefore, the similarity in head forward displacement likely stems from a fortuitous combination of differences.

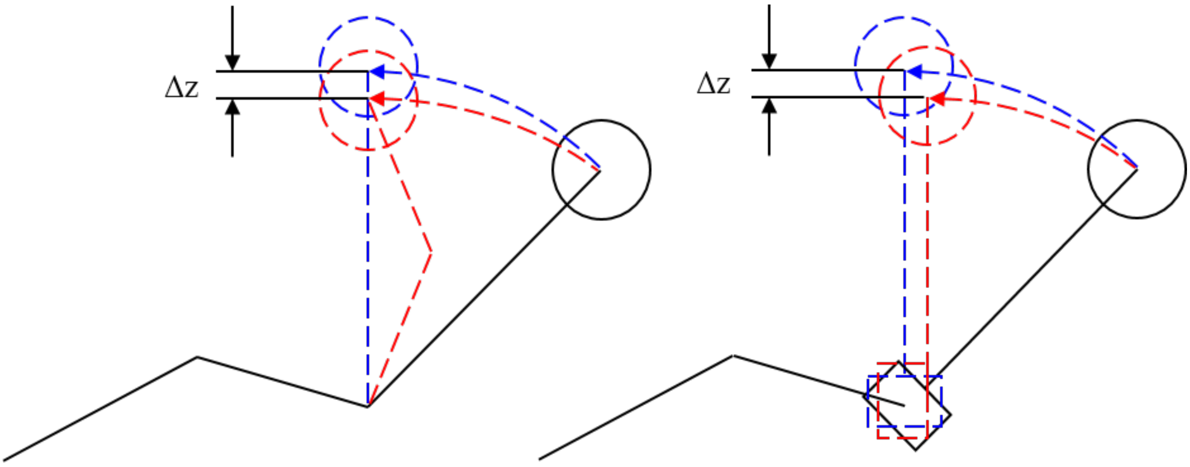

Fig. 10. Principal observed factors in head vertical displacement. Left: a more compliant spine (red) causes the head to move downward compared to a less compliant spine (blue). Right: rearward pelvis rotation (red) moves the head downward while forward pelvis rotation (blue) moves the head upward.

Differences in the ATDs' vertical head displacement may be due to the difference in lumbar stiffness, which subsequently results in pelvis motion (Figure 10, right): assuming the same spine length during the test and amongst the subjects, the THOR-50M's posterior pelvis rotation would displace the head vertically downwards while the HIII-50M's anterior pelvis rotation would displace the head vertically upwards. The difference in head vertical displacement may also be due to the difference in spine stiffness (Figure 10, left): assuming the same pelvis rotation amongst the subjects, the Hybrid-III's greater upward displacement may indicate a stiffer (in compression) spine.

Variation in lateral head motion across the three surrogates was observed (Figure 11). Outboard displacement (displacement in the direction of the D-ring) of the head is expected in frontal impacts with upright occupants restrained by a three-point seatbelt [33] due to the asymmetry of the diagonal shoulder-belt. However, this may not be a valid expectation for reclined occupants, or for occupants restrained by a seatbelt system with lap-belt and buckle pre-tensioners: at the time of maximum forward head displacement, the T1 vertebra moves ~30 mm inboard for the reclined PMHS and ~10 mm outboard for the ATDs. While such small differences in lateral motion of the head and upper spine are inconsequential when set next to the large difference in pelvis motion, future work should not neglect lateral motions due to their implications for shoulder-belt fit, airbag deployment, and vehicle interior interaction risk [34].

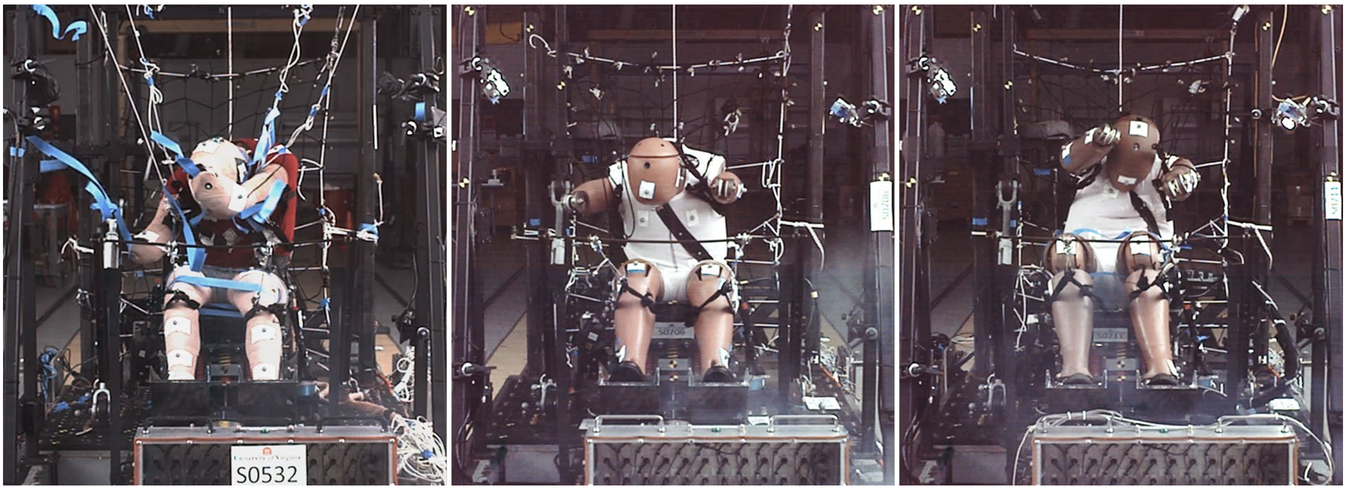

Fig 11. Head kinematics during rebound (t = 170 ms) of PMHS (S0532), HIII-50M (S0706), and THOR-50M (S0711) from left to right.

Interaction between the shoulder-belt and the subject's shoulder may be a potential cause for this variation in lateral head motion. A video analysis showed that the shoulder-belt is further inboard for the THOR-50M than the HIII-50M and the PMHS (Figure 12). For the PMHS and the HIII-50M, the shoulder-belt appears to lie flat along the chest of each subject, while maintaining a consistent distance away from the neck. On the other hand, for the THOR-50M, the shoulder-belt appeared to translate inboard at the neck, slide over the molded shoulder cover, and ride into the cavity between the clavicle assembly and the neck assembly, which may have contributed to the inboard motion of the THOR-50M upon rebound.

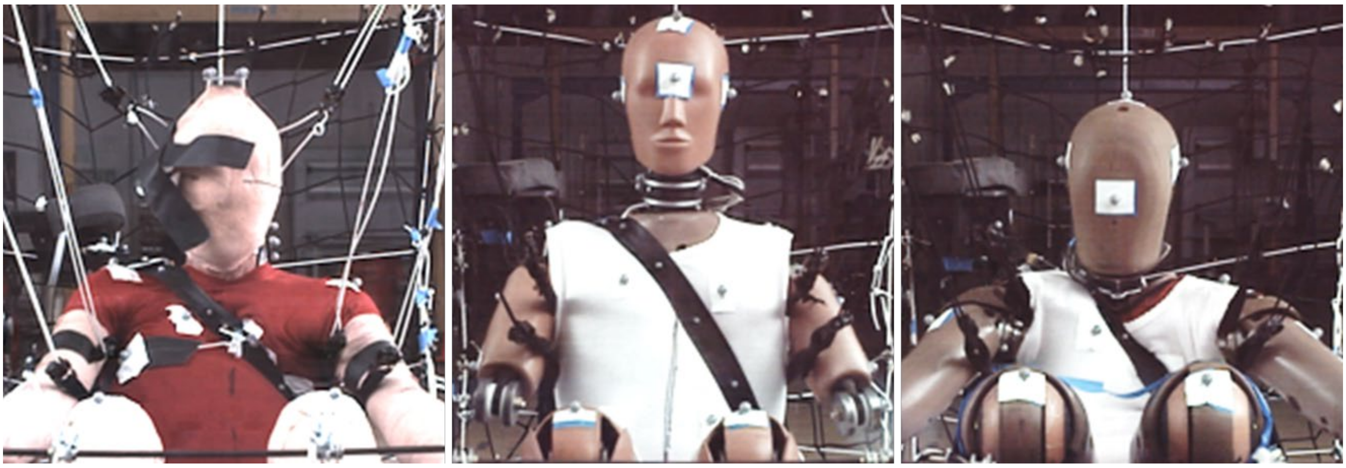

Fig 12. Comparison of shoulder-belt routing across the shoulder and upper torso at 70 ms between PMHS (S0531), HIII-50M (S0706), and THOR-50M (S0711) from left to right.

Despite the differences in head displacement, the THOR-50M exhibits a very similar global head rotation response to the PMHS. This may not, however, indicate biofidelic head and neck behaviour, since the orientation of the upper thoracic spine differed between the THOR-50M and the PMHS: the THOR-50M's T1 trajectory matched that of the PMHS, but its T8 trajectory did not.

Kinematics of the ATDs' heads were measured and transformed to the center of gravity of the head, as defined in the ATDs' user manuals (Appendix A). However, PMHS data regarding the head published in [23] and used to evaluate biofidelity in this paper was measured and transformed to a point corresponding to the midpoint of the zygomatic processes, which may not be an accurate representation of the center of gravity of the head for the PMHS.

Overall, the spine and head motions of reclined subjects seem to depend strongly on spine compliance and pelvis motion. Furthermore, the ATDs may compound dissimilarities in some body regions, i.e., spine and pelvis, to achieve the same kinematic response to the PMHS for another body region, i.e., head. The current analysis highlights a substantial contribution of lumbar stiffness or compliance on resulting kinematics for a reclined condition. Future ATD design and evaluation should consider spine compressive compliance and flexion flexibility as important targets for the reclined occupant response.

V. CONCLUSIONS

In recline, both the HIII-50M and THOR-50M ATDs exhibited comparable responses to the PMHS in some respects, but magnitudes, and even directions, of some specific kinematic parameters varied between the ATDs and the PMHS. Particularly, some substantial differences in pelvis kinematics were observed. As such, ATDs should be further developed to facilitate a more biofidelic response to reclined frontal impact cases. The results of this study indicate that this effort will be best facilitated through a focus on redesigning the pelvic region, as that seems to be where whole-body kinematics begin to diverge. Both ATDs exhibited good repeatability, and largely exhibited responses that straddled the PMHS responses. This study provides detailed data and analysis that could be used in a subsequent study to propose ATD modifications to improve biofidelity.

VI. ACKNOWLEDGEMENTS

The authors would like to thank everyone at the University of Virginia Center for Applied Biomechanics (Charlottesville, Virginia, USA) who assisted with this project. The authors would also like to thank the Research Consortium for Crashworthiness in Automated Driving Systems (East Liberty, Ohio, USA) for funding and the National Highway Traffic Safety Administration (East Liberty, Ohio, USA) and Autoliv (Vårgårda, Sweden) for assisting with this project.

VII. REFERENCES

[1] SAE On-Road Automated Driving Committee. Taxonomy and Definitions for Terms Related to On-Road Motor Vehicle Automated Driving Systems J3016_201401. *SAE International*, 2014.

[2] U.S. Department of Transportation. Automated Driving Systems 2.0 - A Vision for Safety. Available at: https://www.nhtsa.gov/sites/nhtsa.dot.gov/files/documents/13069a-ads2.0_090617_v9a_tag.pdf, September 2017, Accessed February 1, 2022.

[3] U.S. Department of Transportation. Automated Driving Systems 3.0 - Preparing for the Future of Transportation. Available at: https://www.transportation.gov/sites/dot.gov/files/docs/policy-initiatives/automated-vehicles/320711/preparing-future-transportation-automated-vehicle-30.pdf, October 2018, Accessed February 2, 2022.

[4] Östling, M, Larsson A. Occupant activities and sitting positions in automated vehicles in China and Sweden. *26th International Technical Conference on the Enhanced Safety of Vehicles (ESV)*, 2019, Eindhoven, Netherlands.

[5] Jorlöv S, Bohman K, Larsson A. Seating Positions and Activities in Highly Automated Cars – A Qualitative Study of Future Automated Driving Scenarios. *Proceedings of IRCOBI Conference*, 2017, Antwerp, Belgium.

[6] Koppel S, Jiménez Octavio J, Bohman K, Logan D, Raphael W, Quintana Jimenez L, Lopez-Valdes F. Seating configuration and preferences in fully automated vehicles. *Traffic Injury Prevention*, 2019, 20:S103-S109.

[7] Adomeit D, Heger A. Motion Sequence Criteria and Design Proposals for Restraint Devices in Order to Avoid Unfavorable Biomechanic Conditions and Submarining. *SAE Transactions*, 1975, 84(4):3150-3159.

[8] Leung YC, Tarrière C, Lestrelin D, Hureau J, Got C, Guillon F, Patel A. Submarining Injuries of 3 Pt. Belted Occupants in Frontal Collisions – Description, Mechanics and Protection. *SAE Transactions*, 1981, 91(4):3521-3553.

[9] Gepner B, Rawska K, et al. Challenges for Occupant Safety In Highly Automated Vehicles Across Various Anthropometries. *26th International Technical Conference on the Enhanced Safety of Vehicles (ESV)*, 2019, Eindhoven, Netherlands

[10] Rawska K, Gepner B, et al. Submarining Sensitivity across Varied Anthropometry in Autonomous Driving System Environment. *Traffic Injury Prevention*, 2019, 20:S123-S127.

[11] Forman J, Lin H, Gepner B, Wu T, Panzer M. Occupant safety in automated vehicles: effect of seatback recline on occupant restraint. *International Journal of Automotive Engineering*, 2018, 10:139-143.

[12] Kerrigan J, Rawska K, et al. Preventing Submarining for Reclined Occupants of Autonomous Vehicles. *Proceedings of JSAE Annual Congress*, 2019, Yokohama, Japan.

[13] Östling M, Sunnevång C, Svensson C, Kock HO. Potential future seating positions and the impact on injury risks in a Learning Intelligent Vehicle (LIV). *Proceedings of VDI-Tagung Fahrzeugsicherheit*, 2017, Berlin, Germany.

[14] Lin H, Gepner B, Wu T, Forman J. Effect of Seatback Recline on Occupant Model Response in Frontal Crashes. *Proceedings of IRCOBI Conference*, 2018, Athens, Greece.

[15] Mroz K, Östling M, Richardson R, Kerrigan J, Forman J, Gepner B, Lubbe N, Pipkorn B. Effect of Seat and Seat Belt characteristics on the Lumbar Spine and Pelvis Loading of the SAFER Human Body Model in reclined Postures. *Proceedings of IRCOBI Conference*, 2020, Munich, Germany.

[16] U.S. Department of Transportation. Federal Motor Vehicle Safety Standard No. 208; Occupant crash protection. Available at: https://www.ecfr.gov/current/title-49/subtitle-B/chapter-V/part-571/subpart-B/section-571.208, Accessed February 2, 2022.

[17] Hershman L. THE U.S. NEW CAR ASSESSMENT PROGRAM (NCAP): PAST, PRESENT AND

FUTURE. *National Highway Traffic Safety Administration*, 2001, Paper Number 390

[18] Insurance Institute for Highway Safety. Moderate Overlap Frontal Crashworthiness Evaluation Crash Test Protocol Version XIX. Available at: https://www.iihs.org/media/f70ff6eb-d7a1-4b60-a82f-e4e8e0be7323/XPsNNA/Ratings/Protocols/current/test_protocol_moderate.pdf, May 2021, Accessed February 2, 2022.

[19] European New Car Assessment Programme. MPDB Frontal Impact Testing Protocol Version 1.1.2. Available at: https://cdn.euroncap.com/media/67282/euro-ncap-mpdb-testing-protocol-v112.pdf, Accessed March 22, 2022.

[20] Parent D, Craig M, Moorhouse K. Biofidelity Evaluation of the THOR and Hybrid III 50th Percentile Male Frontal Impact Anthropomorphic Test Devices. *Stapp Car Crash Journal*, 2017, 61:227-276.

[21] Albert D, Beeman S, Kemper A. Occupant kinematics of the Hybrid III, THOR-M, and postmortem human surrogates under various restraint conditions in full-scale frontal sled tests. *Traffic Injury Prevention*, 2018, 19:S50-S58.

[22] Richardson R, Donlon JP, et al. Test Methodology for Evaluating the Reclined Seating Environment with Human Surrogates. *26th International Technical Conference on the Enhanced Safety of Vehicles (ESV)*, 2019, Eindhoven, Netherlands.

[23] Richardson R, Donlon JP, et al. Kinematic and injury response of reclined PMHS in frontal impacts. *Stapp Car Crash Journal*, 2020, 64:83-153.

[24] Society of Automotive Engineers. SAE J211-1: Instrumentation for impact test – Part 1 – Electronic instrumentation. 2014.

[25] Shaw G, Parent D, et al. Impact response of restrained PMHS in frontal sled tests: Skeletal deformation patterns under seat belt loading. *Stapp Car Crash Journal*, 2009, 53:1-48.

[26] Parent D, Lessley D, Shaw G, Crandall J. Identification of anatomical landmarks for whole-body kinematic measurement in the THOR Mod Kit frontal impact ATD. *Proceedings of JSAE Annual Congress*, 2012, Yokohama, Japan.

[27] Louden A. Revised THOR 50th Percentile Male Dummy Seating Procedure. *National Highway Traffic Safety Administration*, 2019, DOT HS 812 746.

[28] Moreau D, Donlon JP, et al. A Methodology to Replicate Lap Belt Loading Conditions from a Sled Impact Test in a Non-Impact Dynamic Environment on Whole-Body Postmortem Human Subjects, *Proceedings of IRCOBI Conference*, 2021, Virtual.

[29] Toczyski J, Kim T, Kerrigan J. Methods of updating body orientation in crash scenarios based on body's local angular rate. *Measurement Science and Technology*, 2019, 30.

[30] Perez-Rapela D, Markusic C, et al. Comparison of WorldSID to PMHS kinematics in far-side impact. *Proceedings of IRCOBI Conference*, 2018, Athens, Greece.

[31] Gepner B, Draper D, Mroz K, Richardson R, Ostling M, Pipkorn B, Forman J, Kerrigan J. Comparison of Human Body Models in Frontal Crashes with Reclined Seatback. *Proceedings of IRCOBI Conference*, 2019, Florence, Italy.

[32] Richardson R, Jayathirtha M, et al. Thoracolumbar spine kinematics and injuries in frontal impacts with reclined occupants. *Traffic Injury Prevention*, 2020, 21:S66-S71.

[33] Crandall J, Lessley D, Shaw G, Ash J. Displacement response of the spine in restrained PMHS during frontal impacts. *Proceedings of JSAE Annual Congress*, 2012, Yokohama, Japan.

[34] Donlon JP, Richardson R, et al. Kinematics of inboard-leaning occupants in frontal impacts. T*raffic Injury Prevention*, 2020, 21(4):272-277.

VIII. APPENDIX

APPENDIX A

TABLE AI
ATD STRUCTURE COORDINATE SYSTEM DEFINITIONS

ATD	Structure	Origin	Axes
HIII-50M	*Head*	center of gravity of head	XY-plane aligned with Frankfort plane; X-axis positive anteriorly, Y-axis positive from left to right, Z-axis positive inferiorly
	Spine	center of gravity of upper torso	X-axis perpendicular to Back Upper Plate (P/N 78051-187) (positive anteriorly), Y-axis positive from left to right, Z-axis perpendicular to both X- and Y-axes (positive inferiorly)
	Pelvis	midpoint of left and right H-points	X-axis perpendicular to plane containing right and left ASIS and AIIS (positive anteriorly) (note: plane containing ASIS and AIIS assumed from inspection of drawings to be parallel to plane of Pelvis Instrumentation Cavity); Y-axis positive from left to right; Z-axis perpendicular to both X- and Y-axes (positive inferiorly)
THOR-50M	*Head*	center of gravity of head	XY-plane aligned with Frankfort plane; X-axis positive anteriorly, Y-axis positive from left to right, Z-axis positive inferiorly
	Upper Spine	top right rear corner of right plate of Upper Thoracic Spine Box Weldment (P/N 472-3620)	X-axis along top right edge of right plate of Upper Thoracic Spine Box Weldment (P/N 472-3620) (positive anteriorly), Y-axis positive from left to right, Z-axis along back right edge of right plate of Upper Thoracic Spine Box Weldment (P/N 472-3620) (positive inferiorly)
	Lower Spine	intersection point of top, right, and back planes of Upper Thoracic Spine Flex Joint Bottom Plate (P/N 472-3642)	X-axis along top right edge of Upper Thoracic Spine Flex Joint Bottom Plate (P/N 472-3642) (positive anteriorly); Y-axis positive from left to right; Z-axis along intersection line of right and back planes of Upper Thoracic Spine Flex Joint Bottom Plate (P/N 472-3642)
	Pelvis	midpoint of left and right H-points	X-axis perpendicular to plane containing right and left ASIS and AIIS (positive anteriorly); Y-axis positive from left to right; Z-axis perpendicular to both X- and Y-axes (positive inferiorly)

APPENDIX B

TABLE BI
SELECTED CORRIDOR METHOD FOR EACH BIOFIDELITY EVALUATION RESPONSE

Response	Selected Corridor	Reasoning for Selected Corridor
Seat Force X	NALP	Source signals out of phase
Seat Force Z	NALP	Source signals out of phase
Seat Pan Rotation Y	simple	Source signals in phase
Anti-Sub Pan Rotation Y	simple	Source signals different phase
Footpan Force Resultant	simple	Source signals in phase
Buckle Force Resultant	simple	Source signals in phase
Buckle Displacement Resultant	simple	Source signals in phase
Lap Belt Force	simple	Source signals in phase
Lap Belt Payout	simple	Source signals in phase
Shoulder Belt Force	simple	Source signals in phase
Shoulder Belt Payout	simple	Source signals in phase
Head Displacement X	NALP	Source signals out of phase
Head Displacement Y	simple	Source signals in phase
Head Displacement Z	NALP	Source signals out of phase
Head Rotation Y	NALP	Source signals out of phase
Head ARS Y	NALP	Source signals out of phase
T1 Displacement X	NALP	Source signals out of phase
T1 Displacement Y	simple	Source signals in phase
T1 Displacement Z	NALP	Source signals out of phase
T8 Displacement X	NALP	Source signals out of phase
T8 Displacement Y	simple	Source signals different shapes and in phase
T8 Displacement Z	NALP	Source signals out of phase
T11 Displacement X	NALP	Source signals out of phase
T11 Displacement Z	NALP	Source signals out of phase
L1 Displacement X	NALP	Source signals same shape and in phase
L1 Displacement Z	NALP	Source signals out of phase
L3 Displacement X	NALP	Source signals out of phase
L3 Displacement Z	simple	Source signals different shapes and in phase
Pelvis (H-point) Displacement X	simple	Source signals same shape and in phase
Pelvis (H-point) Displacement Z	simple	Source signals same shape and in phase
Pelvis (H-point) Rotation Y	NALP	Source signals same shape and out of phase
Pelvis ARS Y	simple	Source signals different shapes

APPENDIX C

The positions of the HIII-50M acromia relative to the Clavicle Assembly were calculated using the length of the arm (from shoulder joint center to elbow joint center), an anthropometric study of midsize male upper extremity geometry [A1], and CT-scan measurements of the PMHS.

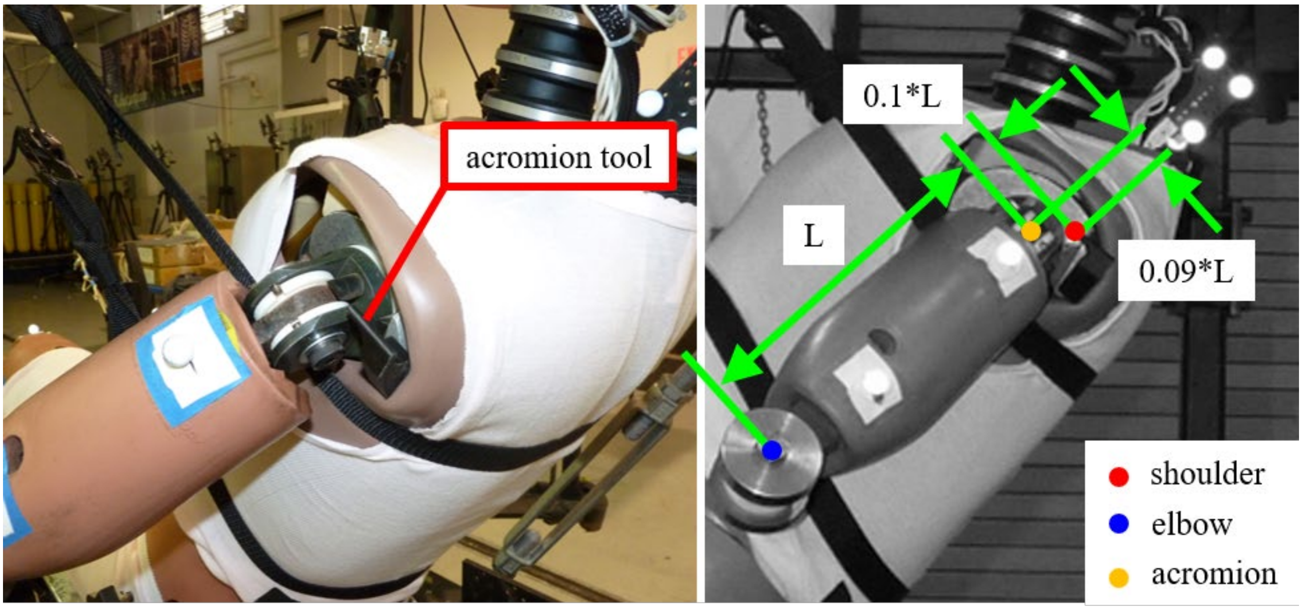

Fig. C1. Acromion Tool for locating the pseudo-anatomic landmark of the acromion relative to the upper arm of the HIII-50M. Left: posterior view of acromion tool installed in shoulder; Right: The acromion position relative to the ATD shoulder was calculated as a function of upper arm length.

APPENDIX D

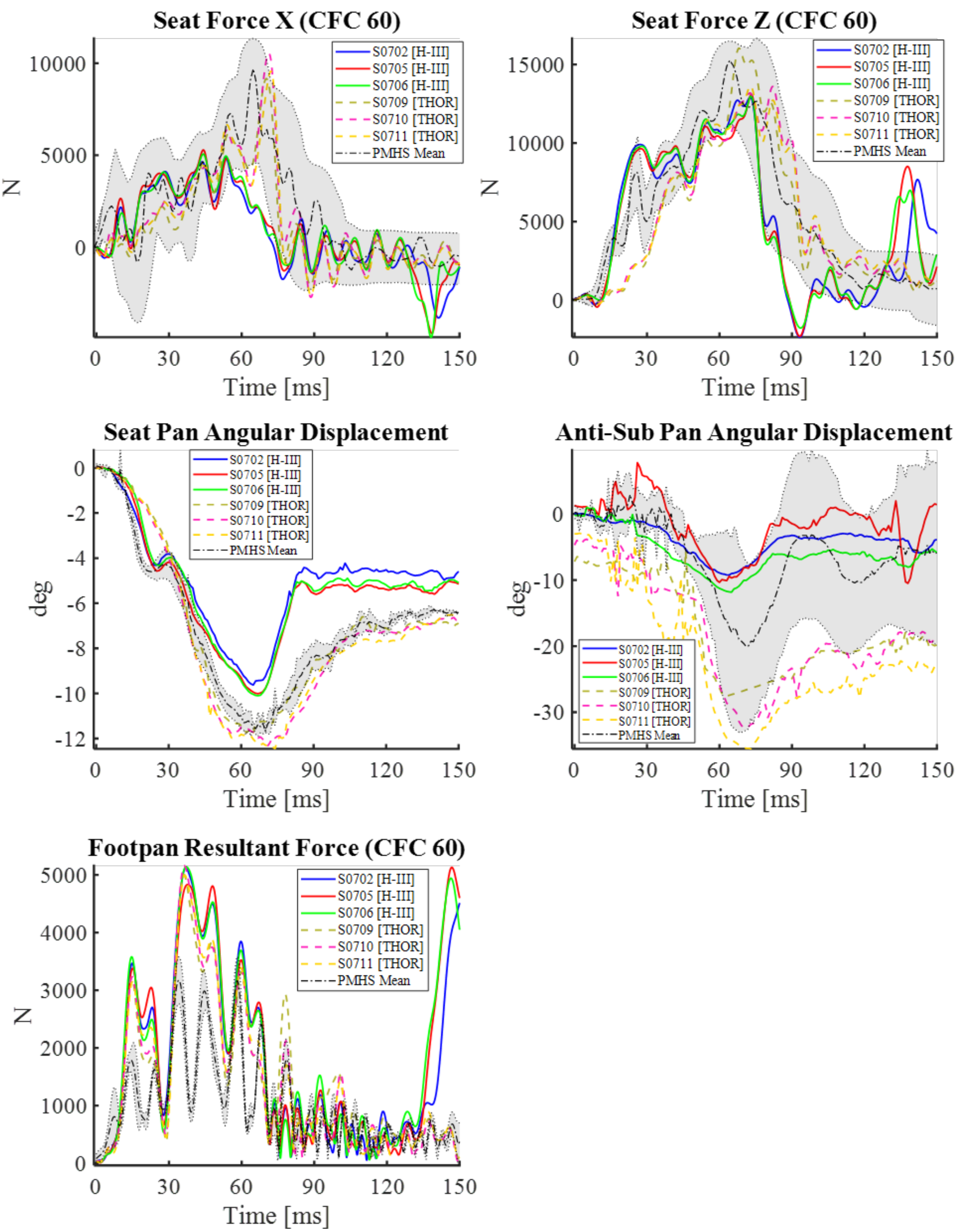

Fig. D1. Seat and footpan kinetics and kinematics

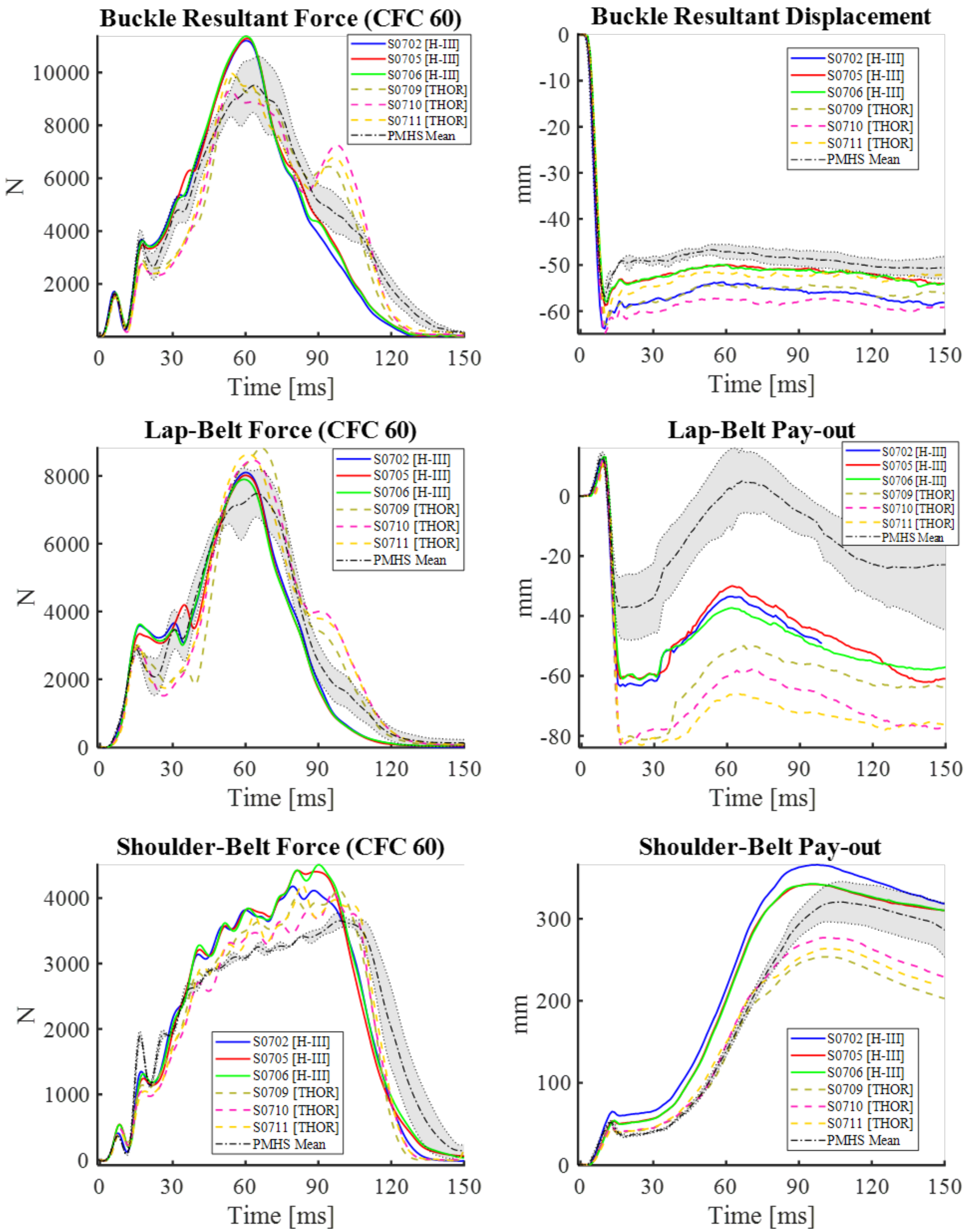

Fig. D2. Restraint components' kinetics and kinematics

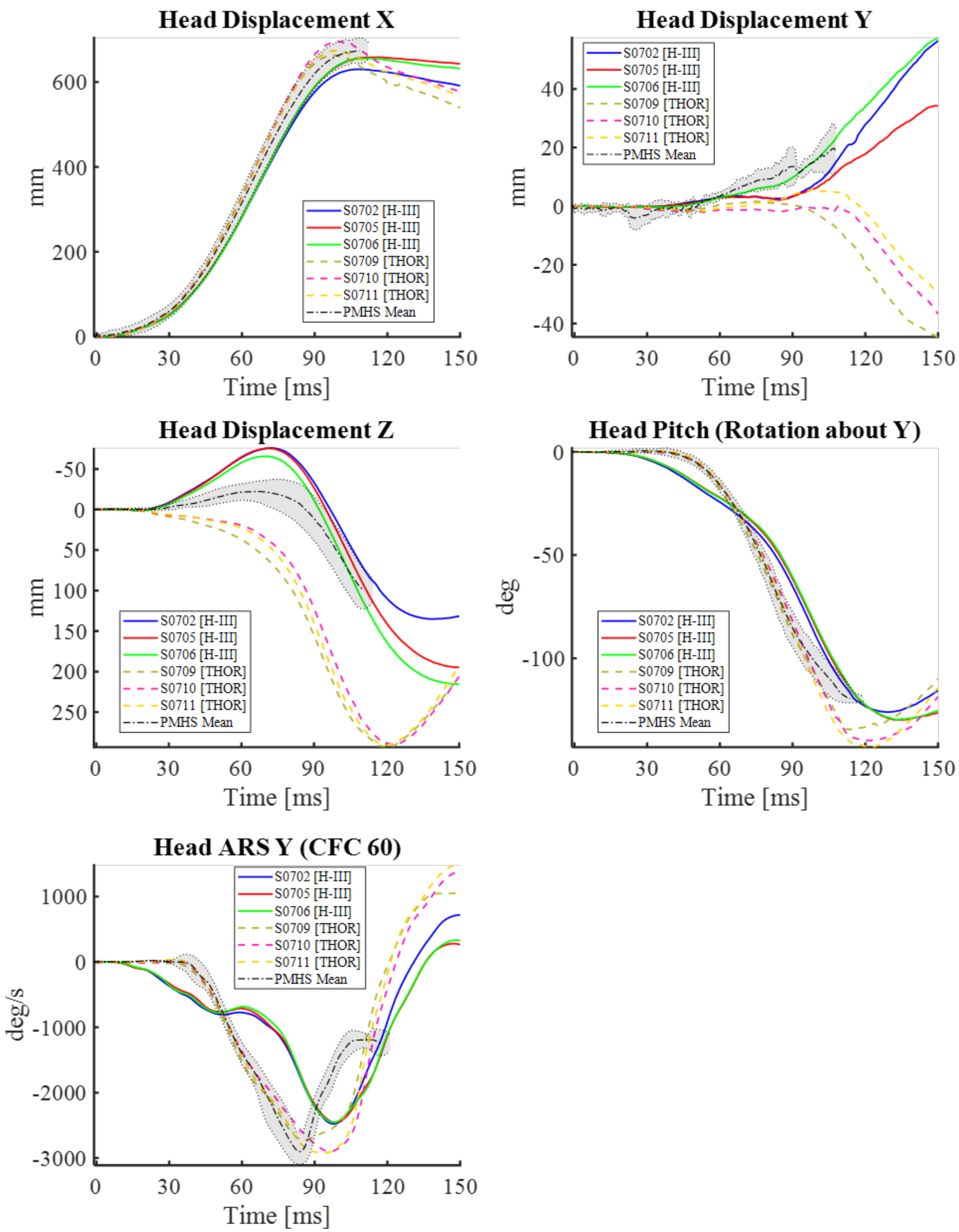

Fig. D3. Head kinematics

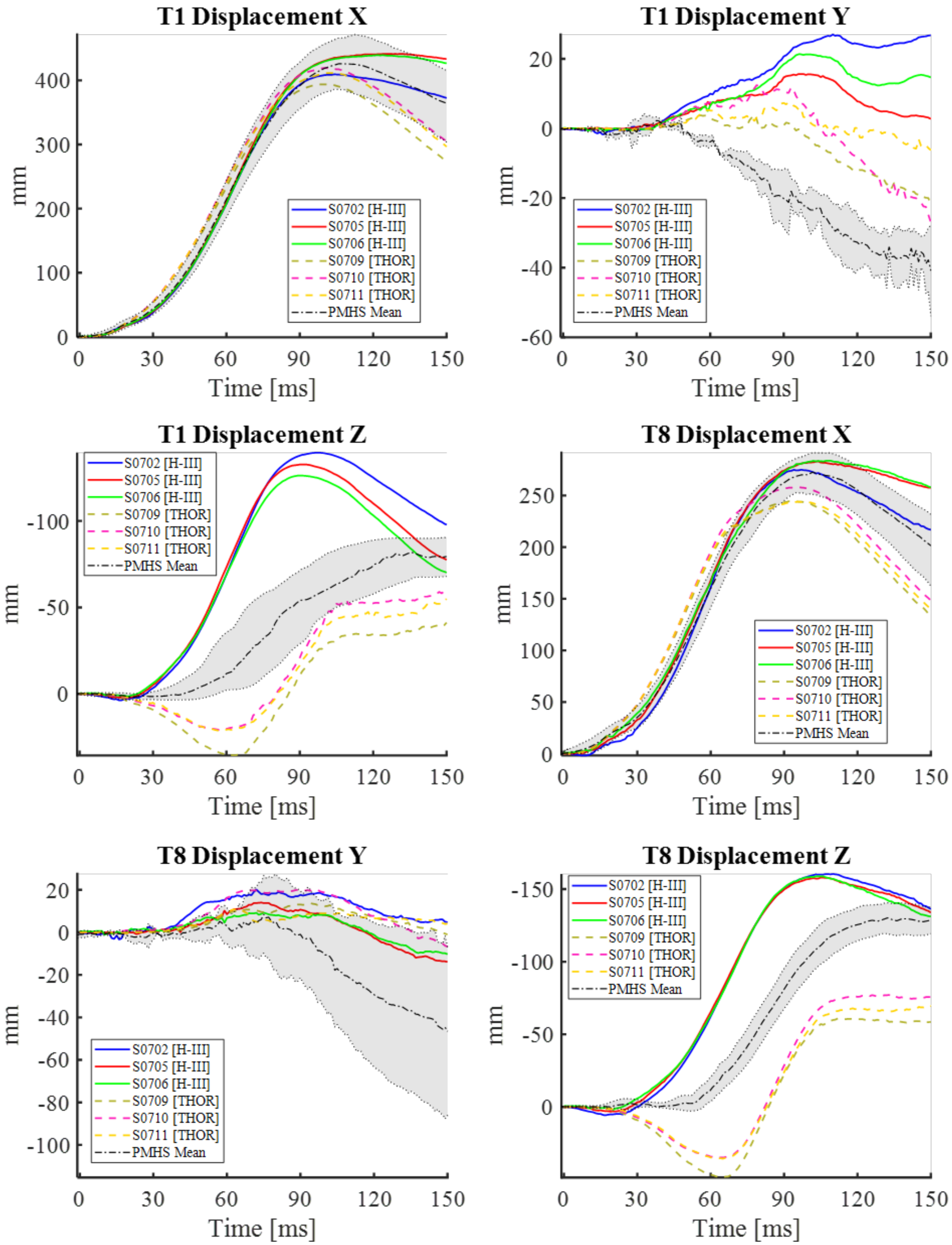

Fig. D4. T1 and T8 kinematics

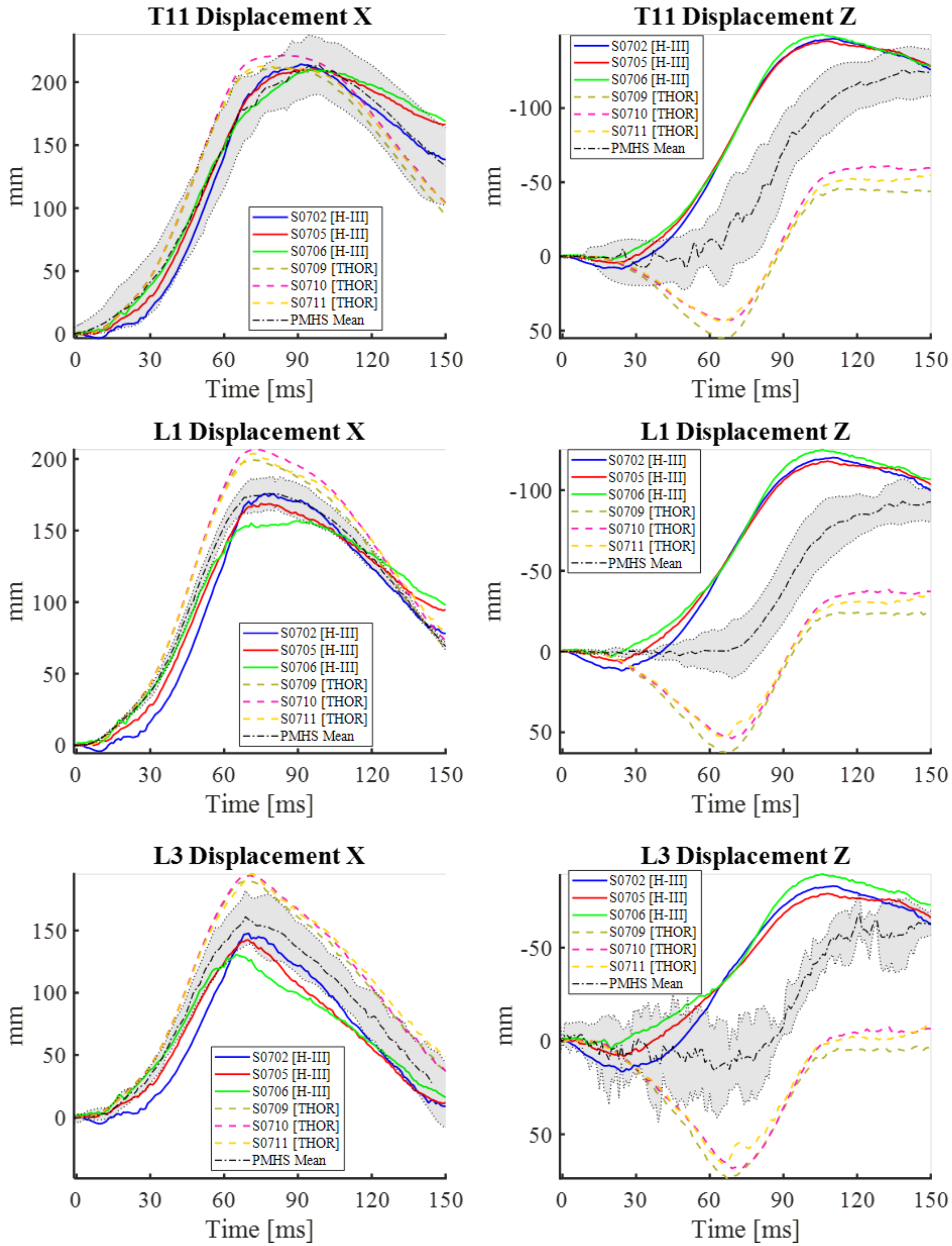

Fig. D5. T11, L1, and L3 kinematics

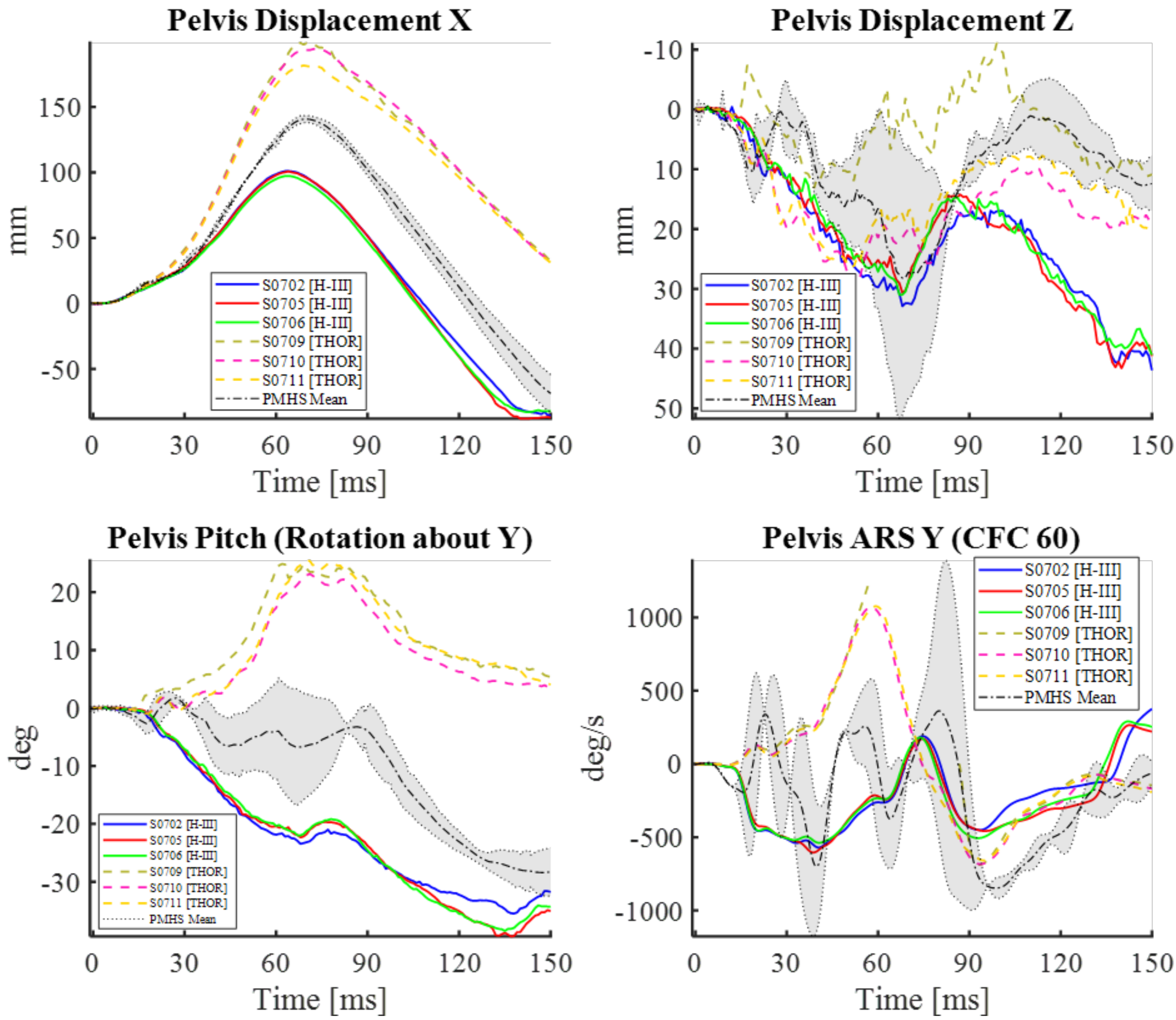

Fig. D6. Pelvis kinematics

APPENDIX E

[A1] de Leva P. Joint center longitudinal positions computed from a subset of Chandler's data. *Journal of Biomechanics*, 2019, 29(9):1231-1233.